Journal of Atmospheric and Solar–Terrestrial Physics 252 (2023) 106147

Contents lists available at ScienceDirect

Journal of Atmospheric and Solar–Terrestrial Physics

journal homepage: www.elsevier.com/locate/jastp

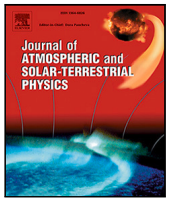

Research paper

# Semidiurnal nonmigrating tides in low-latitude lower thermospheric NO: A climatology based on 20 years of Odin/SMR measurements

Francesco Grieco [a], Yvan Orsolini [b,c,*], Kristell Pérot [a]

[a] Department of Space, Earth and Environment, Chalmers University of Technology, Gothenburg, Sweden
[b] The Climate and Environmental Research Institute (NILU), Kjeller, Norway
[c] Department of Physics, Norwegian University of Science and Technology (NTNU), Trondheim, Norway

ARTICLE INFO

Dataset link: http://odin.rss.chalmers.se/level2

*Keywords:*
Nitric oxide (NO)
Lower thermosphere
Nonmigrating tides
Odin/SMR

ABSTRACT

The Sub-Millimetre Radiometer (SMR) on board the Odin satellite provides almost 20 years of nitric oxide (NO) measurements in the mesosphere and lower thermosphere (MLT) at equatorial crossing local solar times (LSTs) of 6 AM and 6 PM. In this study, we use Odin/SMR observations to estimate how lower thermospheric NO mixing ratios at low latitudes are affected by solar nonmigrating tides. Most of the previous studies based on satellite data have focused on the signatures of diurnal tides in the MLT and above, while we concentrate here on nonmigrating semidiurnal tides. To study the contribution of these tides to NO mixing ratio variations, we average pairs of NO measurements along ascending and descending orbital tracks at 107 km altitude over latitudes between −40° and +40°. We consider monthly climatologies of these pair-averages and analyse residuals with respect to their zonal mean. In this way, it is possible to study the effect of nonmigrating even-numbered tidal components, albeit there is a non-tidal component arising largely from quasi-stationary planetary waves. Spectral wave amplitudes are extracted using a Fourier transform as function of (apparent) zonal wavenumber with a focus around −30°, −20° and 30° latitudes. From our analysis, it appears that the semidiurnal (apparent) zonal wavenumber 4 arising from the SW6 and SE2 tides is dominant close to the equator (e.g., at −20°), except during some boreal summer months (June, July, August). On the other hand, wave-1 plays a more prominent role at subtropical latitudes, especially in the southern hemisphere, where it surpasses wave-4 during 7 months (March and May-to-October) at −30°. There is little observational evidence to date documenting the presence of the semidiurnal nonmigrating tides in NO in the low-latitude MLT. Our results hence provide one of the first evidences of the climatological signature of these tides in NO, in an altitude range that remains poorly observed.

## 1. Introduction

Solar atmospheric tides are planetary-scale inertia-gravity wave oscillations with periods corresponding to the 24-hour solar forcing and its sub-harmonics. They manifest in dynamical quantities like temperature, horizontal or vertical winds, density, as well as in various trace constituents. These tides can either be migrating – i.e. moving westward following the apparent motion of the Sun – or nonmigrating — i.e., propagating eastward, or westwards but not synchronously with the Sun, or even non-propagating as standing zonally symmetric time oscillations. The source of migrating solar tides is primarily the absorption of solar radiation by water vapour in the troposphere, by ozone in the stratosphere, and by atomic and molecular oxygen or nitrogen in the thermosphere (for a review Oberheide et al. (2015), Sakazaki et al. (2015)). Zonal asymmetries in ozone and water vapour and in large-scale latent heat release in convective cloud systems in the tropical troposphere are the key forcings of nonmigrating tides (Lieberman, 1991; Oberheide et al., 2002; Hagan and Forbes, 2003; Liu et al., 2018). The zonally asymmetric latent heating pattern is imparted by the continent geography constraining large-scale convection at low latitudes. Nonlinear interactions between tides or between migrating tides and quasi-stationary or travelling planetary waves (PW) also contribute to the generation of nonmigrating tides (Pancheva et al., 2002; Truskowski et al., 2014; He et al., 2017; Zhang et al., 2021, and references therein). Tides also interact with gravity waves (McLandress and Ward, 1994), modulating their vertical propagation. In turn, the latter modulate tidal amplitudes, contributing to their day-to-day variability.

While of relatively minor importance in the lower atmosphere, solar tides strongly contribute to the variability of the mesosphere and lower thermosphere (MLT) and the ionosphere–thermosphere (I–T) from daily

* Corresponding author at: The Climate and Environmental Research Institute (NILU), Kjeller, Norway.
*E-mail address:* yor@nilu.no (Y. Orsolini).

https://doi.org/10.1016/j.jastp.2023.106147
Received 22 February 2023; Received in revised form 21 August 2023; Accepted 30 September 2023
Available online 7 October 2023

to seasonal timescales (Oberheide et al., 2011; Liu et al., 2018). As such, atmospheric tides have been shown to play an essential role in the coupling between the tropospheric weather and space weather in the MLT region and further above in the I-T.

In standard tidal nomenclature, tides are identified by a series of letters and numbers indicating their period, propagating direction and zonal wave number. For example, DW2 indicates a diurnal (D) tide propagating westward (W) and with a zonal wave number of 2, whereas SE1 indicates a semidiurnal (S) tide propagating eastward (E) and with a zonal wave number of 1. The main migrating tides are DW1, SW2 and TW3, T standing for terdiurnal. While some tides remain trapped near their source region, some can propagate upward and, due to the decrease of density with altitude and the conservation of energy, increase in amplitude until they reach the thermosphere where they dissipate due to molecular and eddy diffusion or radiative damping, releasing heat and momentum. Vertical propagation and dissipation depend on the vertical wavelength, with tides of shorter wavelength undergoing more dissipation and tides of very long wavelength having their vertical propagation hindered by the "mesospheric barrier" (Truskowski et al., 2014). The filtering by the background thermal structure, by mean winds and by the wave-wave interactions play important roles in modulating tidal amplitudes. Migrating tides tend to provide the dominant signature, but nonmigrating tides (especially, if combined) can become as large as migrating tides at certain times of year and in some altitude ranges (Oberheide et al., 2002; Lieberman, 1991). Note that not all tides in the MLT do propagate from below, as they can also be generated in-situ in the thermosphere due to the absorption of far-ultraviolet solar radiation and geomagnetic effects.

Of particular interest for the thermosphere are the tidal impacts on nitric oxide (NO), which affects the thermospheric infrared cooling rate and energy budget (Bermejo-Pantaleón et al., 2011; Ren et al., 2020). Some satellite observations allow retrieving NO abundance: for example, the Student Nitric Oxide Explorer (SNOE) instrument measured NO abundance at a single local solar time (LST) in daylight between March 1998 and September 2000. Based on these observations, Oberheide and Forbes (2008) found waves-3 and −4 signatures in lower thermospheric NO, which they showed to be –to a large extent– manifestations of the DE2, DE3 and SE1 nonmigrating tides. Diurnal variations of NO at low latitudes due to migrating tides have also been studied using observations from the SNOE and from the Solar Occultation For Ice Experiment (SOFIE) instrument e.g., Marsh and Russell III, 2000; Siskind et al., 2019. Other instruments like the Sounding of the Atmosphere using Broadband Emission Radiometry (SABER) measured NO volume emission. The tidal fluctuation in NO is the result of several drivers (temperature, density and advection). Hence, the tidal impact on NO volume emission or NO cooling rate is more complex and convolves the effects of the tidal fluctuations in temperature, density, as well as tidal advection of the mixing ratio of NO, and to a lesser extent, of other species like atomic and molecular oxygen (Ren et al., 2020). This is due to the fact that NO can vary through the tidal temperature fluctuation (as the NO chemical production and loss are temperature-dependent), or density fluctuation, but also through tidal vertical advection (since NO has a large vertical gradient in the MLT). Based on SABER data analysis and photochemical modelling, Nischal et al. (2019) demonstrated that the DE2 and DE3 also impact the NO cooling rate, which peaks near 130–140 km. These two tides, originating in the troposphere, attain large amplitudes in the I–T at low latitudes, with DE3 being the largest and exceeding even the amplitude of migrating tides (Liu et al., 2018). Observational and model studies from Ren et al. (2020) and Nischal et al. (2019) suggested that the principal influence of DE3 and DE2 on the NO cooling rate at low latitudes arises through temperature up to 110 km, before the density fluctuations start contributing.

Constraining the amplitude of diurnal NO variations, whether tidal or chemical, is fundamental to study chemical and dynamical processes occurring at these altitudes and to allow comparisons of measurements made by different satellite instruments taken at different LSTs. The Sub-Millimetre Radiometer (SMR) aboard the Odin satellite observes the middle atmosphere along about 14 orbits each day with equatorial crossing times of 6 am and 6 pm LST along its descending and ascending tracks, respectively. As of today, these LSTs are different from all other satellite instruments observing NO in the MLT, allowing to further constraint the amplitude of NO diurnal variations. Moreover, it provides one of the most extended MLT NO data sets, covering almost 20 years of measurements. The aim of this study is to use NO retrieved by Odin/SMR to estimate how and to what degree the variations in NO mixing ratios in the lower thermosphere at low latitudes are affected by nonmigrating semidiurnal tides. While it is recognized that tidal amplitudes can vary on a day-to-day timescale, with their daily variability as high as half of their total variability (Kumari, 2021), we only consider their climatological signature on NO in this study. With a focus on low latitudes, we also neglect day-to-day NO fluctuations due to geomagnetic activity, which tend to occur mostly at high latitudes, albeit soft X-rays variations during geomagnetic storms may impact low latitudes. While many of the aforementioned studies have highlighted the important signatures of the nonmigrating diurnal tides (like DE2 and DE3), less attention has been devoted to the impact of nonmigrating semidiurnal tides. Nevertheless, these semidiurnal nonmigrating tides were previously observed aloft in the thermospheric densities observed by satellite at 144 and 332 km, along with the diurnal tides DE2 and DE3 by Bruinsma and Forbes (2010). More recently, Forbes et al. (2022) observed a variety of semidiurnal nonmigrating tides in the thermospheric wind observations made between 100 and 280 km during the year 2020 by the MIGHTI (Michelson Interferometer for Global High-resolution Thermospheric Imaging) instrument. They highlighted the need to understand their generation and propagation through the thermosphere. Concerning NO more specifically, Oberheide and Forbes (2008) pointed out that, at the equator, semidiurnal nonmigrating tides appear prominently in NO during the boreal winter. The aim of this paper is to present a climatology of nonmigrating semidiurnal tides as seen in 20 years of NO observations by the Odin/SMR instrument. The instrument and the method used in this study are presented in Section 2. In Section 3, we present our estimates on the contribution of the various semidiurnal nonmigrating tidal components on NO mixing ratio diurnal variation. In Section 4, we discuss the results and compare them with other studies.

## 2. Odin/SMR data set and analysis

The Odin satellite was launched on 20 February 2001 into a 600 km sun-synchronous orbit with an inclination of 97.77° and a 6 PM ascending node. The Sub-Millimetre Radiometer (SMR) on board the satellite performs limb sounding of the middle atmosphere through its four sub-millimetre receivers which cover frequencies between 486–504 GHz and 541–581 GHz, and a millimetre receiver measuring around 118 GHz. The observed bands allow to detect radiation from rotational transitions of different chemical species, among which is nitric oxide (NO) with its two thermal emission lines at 551.48 and 552.05 GHz (Eriksson, 1999; Frisk et al., 2003). The instrument observational time was shared between astronomical and atmospheric observations until 2007. Atmospheric NO measurements were then carried out one day per month. After that, the instrument has been entirely employed for atmospheric observations and so is still today, with NO being measured 4–5 days per month. The number of NO measurement days per month has been occasionally increased during dedicated observational campaigns (Pérot and Orsolini, 2021). SMR NO measurements cover latitudes between −82.5° and 82.5° and altitudes between 45–50 km and 110–115 km, with a vertical resolution of 7 km. Version 3.0 of SMR level 2 NO data, resulting from a recent reprocessing of the data set, are used in this study. No proper validation study has yet been performed for this data set. However, agreement with other instruments such as SOFIE, SCIAMACHY (SCanning Imaging

Absorption spectroMeter for Atmospheric CHartographY), ACE-FTS (Atmospheric Chemistry Experiment-Fourier Transform Spectrometer) and MIPAS (Michelson Interferometer for Passive Atmospheric Sounding) was found by carrying out a comparison regarding variability in MLT NO concentration, using simulations from an empirical model based on SMR v3.0 measurements (Kiviranta et al., 2018). This showed the reliability of the data set.

Sun-synchronous satellite take observations at fixed local times and, in this fixed local time reference frame, tides of zonal wavenumber k (k = 0, k > 0 and k < 0 correspond to standing, westward propagating and eastward propagating oscillations, respectively) manifest at an apparent wavenumber |k-n|, where n is an integer denoting the subharmonics of the planetary rotation period (e.g. n = 1 for diurnal, n = 2 for semidiurnal). For example, it is well established that the DE3 tide (n = 1 and k =−3) largely contributes to the apparent wave-4 structure seen in sun-synchronous satellite observations in the MLT during certain months (Oberheide and Forbes, 2008; Liu et al., 2018). In this frame, migrating tides also appear to be longitude-independent. Several studies (Lieberman, 1991; Oberheide et al., 2013; Liu et al., 2018; García-Comas et al., 2016) combined pairs of observations, taken 12 h apart in local time along ascending and descending orbital tracks: their difference cancels out even-number (semidiurnal and quarterdiurnal) tides preserving the odd-number (diurnal and terdiurnal) tides (García-Comas et al., 2016). On the other hand, their average cancels out the latter but preserves the contribution of the former, together with the contribution of a non-tidal signal. The latter notably comprises quasistationary PWs (QSPWs) which contribute to the spectrum at their actual wavenumber (k), a contribution which would cancel out if taking the orbital tracks difference.

A spectral analysis of the observed longitudinal structure then allows to extract the tidal amplitudes for each apparent zonal wavenumber. Note that several tidal components are contributing to the same apparent wavenumber. For example, when taking orbital track average, several even-number nonmigrating tides (either westward or eastward-propagating) are contributing to the same apparent wavenumber: Table 1 summarizes all the major semidiurnal nonmigrating tidal components as well as the QSPWs contributing to each apparent zonal wavenumber. Quarterdiurnal tides are not included because they are generally of small amplitudes at low latitudes (Smith et al., 2004), appearing mostly during special occurrences at mid and high latitudes such as during stratospheric sudden warmings when tide–tide nonlinear interaction might be important. See García-Comas et al. (2016) for a corresponding table for odd-number tides when taking the orbital tracks difference. The wavenumber 0 contains the contribution of the migrating tide as well as a longitude-independent background, while higher wavenumber contributions represent nonmigrating tides.

In this study, monthly climatologies obtained by averaging pairs of ascending (LST ∼ 6 PM) and descending (LST ∼ 6 AM) measurements are calculated based on the whole Odin satellite observation period. One ascending and one descending measurements constitute a pair if they occur in the same bin within 24 h. We base our study on 107 km altitude data because this altitude corresponds to a region of the atmosphere where the NO mixing ratios are close to their maximum (Siskind et al., 1998) and where the effects of tides are known to be important (Siskind et al., 2019). The data corresponding to 107 km altitude are averaged over bins which are 24° wide in longitude and 15° in latitude, over a domain spanning around 40° latitude on each side of the equator. The size of the bins in longitude has been chosen so that one full day of observations (e.g. along 14 orbits) would populate each bin with one pair of observations. Moreover, we focus on bins from −20° to ±30° latitude to be able to study a greater number of measurements than in the equatorial region, since only a small amount of level-2 SMR NO data is available in the °0 – +10° latitude area, due to failures in the retrieval process.

Our focus is on the monthly climatology of the averages of each pair of measurements (that is (AM + PM)/2, hereafter referred to as pair-average), which is calculated as follows for each month: given a latitude–longitude bin, we calculate the all pair-averages in the bin over the years, and then calculate the total median; after doing this for each longitude bin, we express this quantity in form of a residual by subtracting and dividing by the zonal mean. This way we obtain, for each longitude bin, the deviation in percentage of pair-average NO mixing ratio from the zonal mean. Since the solar migrating tides are longitude-invariant, considering the residual (that is, subtracting the zonal mean) allows us to study zonal variability in NO mixing ratios which is only due to nonmigrating tides and the non-tidal component. Finally, by applying a fast Fourier's transform (FFT), we can estimate the amplitudes of the waves which contribute to the zonal variation in the NO abundance at 107 km and at several latitudes, as a function of the apparent zonal wavenumber (with $|k-n| \neq 0$, since 0 represents the zonal mean). Given the irregular sampling of the SMR NO observations, limited to a few non-consecutive days per month, we focus on their climatological amplitudes.

**Table 1**
Main nonmigrating tides and QSPWs contributing to the various spectral components extracted from pair-average NO mixing ratio oscillations. Quarterdiurnal tides are not included because of their small amplitudes.

| Apparent wavenumber \|k-n\| | Components |
|---|---|
| 1 | SW1 + SW3 + QSPW1 |
| 2 | SW4 + S0 + QSPW2 |
| 3 | SW5 + SE1 + QSPW3 |
| 4 | SW6 + SE2 + QSPW4 |
| 5 | SW7 + SE3 + QSPW5 |
| 6 | SW8 + SE4 + QSPW6 |

An overview of the number of pairs of measurements at 107 km altitude and −20° latitude used in this study, for each year and month, is presented in Fig. 1a. Similar numbers of pairs pertain to −30° and 30° latitudes (not shown). The values shown consist of the means over all longitude bins. The values roughly represent the number of complete observation days over the months and years, since complete orbital coverage on a given day populates each bin with one pair. Note that the SMR NO observations are not carried out uniformly throughout the years, as mentioned above, and that there are no measurements performed during northern summers from 2013 onwards because the instrument was put in standby mode when the sun is eclipsed by the earth, disabling solar panels while the aged batteries are not sufficient to power the instrument. For this reason, tidal amplitudes extracted during these months are almost entirely obtained from measurements taken during years 2007 and 2012. Also note that when the AM and PM measurements are not taken exactly 12 h apart, due to orbit precession for example, there is a cross-contamination of the odd and even tidal components. Fig. 1b shows that the vast majority of the time separations between all the pairs in the latitude band −30° and 30°, is indeed 12 h and that all departures are within an half-hour. For such small time separations, the relative cross-contamination from diurnal tides involve factors like $\cos(\pi \cdot \frac{11.5}{12})$, and remains with 1 or 2 percent. For semidiurnal tides, the corresponding factor is $\cos(2\pi \cdot \frac{11.5}{12})$ and the relative cross-contamination could increase to 4 percent. We note that the departure from 12 h is more pronounced during the boreal summer.

In order to support the results about semidiurnal tidal signatures in NO, the monthly pair-averaging analysis was repeated on SMR mesospheric temperature measurements (version 3.0) ranging from 50 to 95 km, over the same years and with the same temporal distribution of measurements as for NO, at least after 2007.

## 3. Results

Figs. 2a, 2b and 2c present the monthly climatologies of the nonmigrating semidiurnal tidal amplitudes as a function of the apparent zonal wavemuber, extracted through Fourier's transform of pair-average monthly medians at 107 km altitude. These are shown for

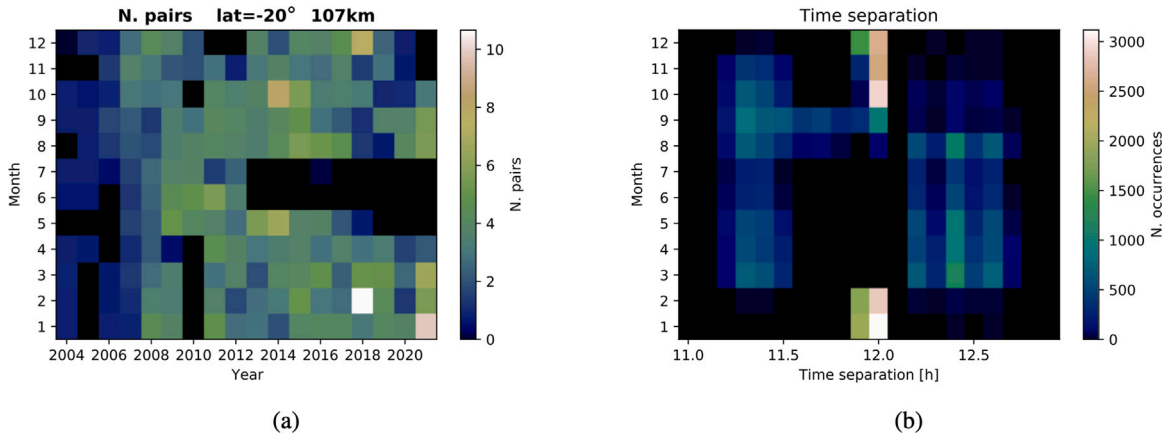


**Fig. 1.** **(a)** Number of ascending/descending pairs of SMR NO measurements, in each latitude–longitude bin at 107 km altitude and −20° latitude, for each year and month, averaged over all longitude bins. **(b)** Time separation of all ascending/descending pairs at latitudes −30°, −20° and +30°. The colours represent the number of occurrences of each value. (For interpretation of the references to colour in this figure legend, the reader is referred to the web version of this article.)

−30°, −20° and 30° latitudes respectively. Wave components with an apparent wavenumber higher than 6 are not shown because they are of negligible amplitude. Each monthly amplitude is presented as a percentage residual with respect to the relative zonal mean. The monthly evolution in Fig. 2b shows that the semidiurnal wave-4 component is dominant except around boreal summer months at −20°. Its amplitude reaches a maximum of 19% during November and a minimum of 4% during June. On the other hand, it appears that the wave-1 component is dominant during boreal summer months with its amplitude maximum in June when it reaches a value of 19%, and minimum in January with a value of less than 5%. In Fig. 2a, at −30°, the wave-1 component is dominant during a more extended period, including not only the summer months but also March, May, September and October. The wave-4 even weakly surpasses the wave-1 in February. In Fig. 2c, at 30°, wave-4 is again dominant, except in August, September and October.

It also appears that other apparent wavenumbers also occasionally contribute significantly during given months, such as the wave-2 and −3 components in June when their amplitudes are around 10% and 7%, respectively, at −20° (see Fig. 2b).

The zonal mean value, corresponding to the |k-n|=0 component, depends on various contributions among which are the migrating tide SW2 and the background NO mixing ratio value (around which oscillations due to migrating tides occur). Its monthly climatology is represented in Fig. 3 for −20° latitude. The zonal mean monthly climatologies for −30° and 30° latitudes are not shown because they are similar to the one shown in Fig. 3. The seasonal amplitude is characterized by a maximum in August–September, a minimum in March, and a secondary maximum in boreal winter. The peak in August and the minimum in March at −20° latitude is consistent with SABER observations of the temperature SW2 tide (Truskowski et al., 2014). Peak values in August and in boreal winter are consistent with the model results of Salinas et al. (2023) for the SW2 tide in temperature at low latitudes near 110 km.

A monthly climatological view of the pair-average residuals spanning the −40°–+ 40° latitude region, is shown at 107 km altitude in Fig. 4. Confirming the conclusions drawn from Fig. 2, it appears that the wave-4 component is dominant closer to the equator except in the boreal summer, when the wave-1 predominates, and that the latter is more prominent at subtropical latitudes, especially in the southern hemisphere. In the northern hemisphere subtropics, there is a relative paucity of measurements, as mentioned in Section 2.

## 4. Discussion and conclusions

There are very few other satellite instruments measuring NO to allow a comparison with our results. Comparing with the SABER-derived NO volume emission or cooling rate is not as straightforward for the reasons discussed in the Introduction. Some correspondence with tidal signature in SNOE-based NO densities should be expected. Unfortunately, the study of Oberheide and Forbes (2008) was limited to the equator where the SMR coverage is limited.

The climatologies of the main nonmigrating semidiurnal tides and of QSPWs near 110 km across low latitudes, as derived from SABER temperature observations over the period 2002–2010 in Truskowski et al. (2014) demonstrate that the QSPWs have a weak signature within 20 degrees of the equator, except for the wave-2 in the southern hemisphere subtropics in March-April. However, a QSPW4 has been reported previously in wind observations in the low-latitude thermosphere (Oberheide et al., 2011; Forbes et al., 2022). With these exceptions in mind, QSPWs can therefore be neglected in the following analysis.

Our first main result concerns the dominant nonmigrating semidiurnal wave-4 signature except during some boreal summer months (June, July, August, September) at −20°. The apparent wave-4 might arise from the SW6 and SE2 tides (see Table 1). On the other hand, wave-1 plays a more prominent role at subtropical latitudes, especially in the southern hemisphere, where its surpasses wave-4 during 7 out of 12 months (March and May to October) at −30°. Even in winter, the contribution from wave-4 is only slightly greater than the contribution from wave-1 at that latitude. At 30°, wave-1 surpasses wave-4 from August to October, and remains comparable or smaller by a factor 2 during the other months. This dominance of wave-4 in boreal winter is roughly consistent with Nischal et al. (2019) who calculated the nonmigrating semidiurnal tide signature in NO cooling rate over the −40°–+ 40° latitude band for December 2013 at 125 km, and revealed the importance of SW6 and SE2. The detailed seasonal evolution for the solar minimum year 2008 in Nischal (2019) also revealed that this SW6 tide maximized in relative amplitudes at between 7 and 12% in January–February near 107 km at −30°, making it comparable to our climatological relative amplitudes (see Fig. 2a).

Both SW6 and SE2 could be generated in the troposphere by the semidiurnal modulation of latent heating combined with the zonal wavenumber 4 imparted by the continent geography. This is suggested by the linear modelling in Truskowski et al. (2014), Hagan and Forbes (2003), Zhang et al. (2006), who showed that these two tides in

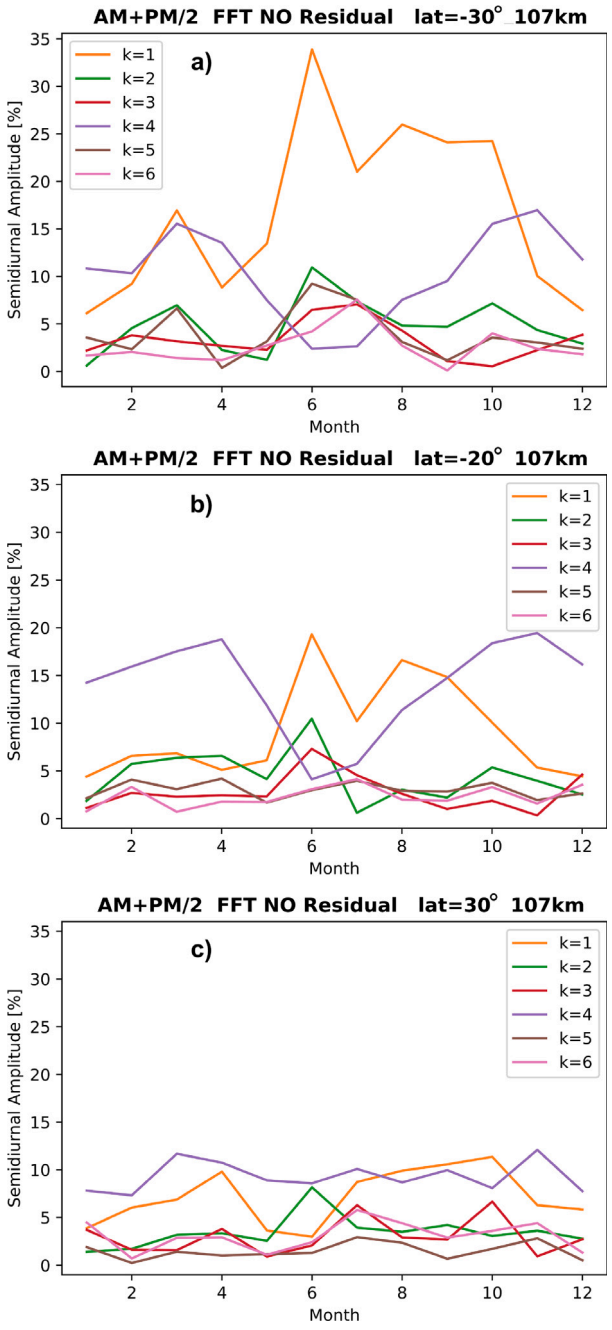


**Fig. 2.** Residual semidiurnal tidal amplitudes as a function of apparent zonal wavenumber extracted from monthly climatologies of SMR pair-average NO mixing ratio at 107 km altitude and −30° (a), −20° (b) and 30° (c) latitude. Percentage values are referred to the corresponding monthly zonal means, as presented in Fig. 3 for the latitude of −20° for example. The components with an apparent wavenumber higher than 6 have a negligible amplitude and are therefore are not shown.

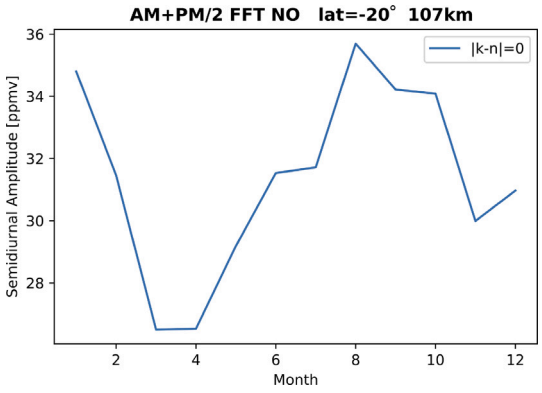


**Fig. 3.** Zonal mean ($|k-n|=0$ component) extracted from monthly climatologies of SMR pair-average NO mixing ratio oscillations at 107 km altitude and −20° latitude.

temperature in the MLT were forced by both latent and radiative heating. The shorter vertical wavelength of SW6 compared to SE2 (46 vs 77 km (Truskowski et al., 2014)) makes it more susceptible to dissipation before it reaches the MLT. Another possibility is in-situ generation in the MLT through non-linear tide–tide interaction involving the DE3 and DW1 tides, thereby generating QSPW4 and SE2. Subsequently, the non-linear interaction of QSPW4 with the background SW2 would be generating SW6 and SE2 (Nischal, 2019; Oberheide et al., 2011). Note that all the "child products" of these non-linear interactions (QSPW4, SE2 and SW6) correspond to an apparent wave-4 (see Table 1) and would be indistinguishable in our analysis.

Further analysis of the semidiurnal nonmigrating tides in SMR mesospheric temperatures (from 50 to 95 km; Fig. 5) reveals a prominent apparent wave-4 in December, January, and February above 85 km but not below, supporting the tidal signature seen aloft in NO, but also indicating that a lack of propagation through the stratosphere. This argues for an in-situ origin of the apparent wave-4 semidiurnal signature. However, the precise mechanism remains unknown, since the generation process outlined above would be expected to operate during boreal summer, as it starts with a strong DE3 presence. Investigations of the possible mechanism likely require supporting model studies.

The second finding concerns the apparent wave-1 which dominates in boreal summer at −20°, and during other months as well at subtropical latitudes. The apparent wave-1 might arise from the westward tides SW3 and SW1 (see Table 1). This is also roughly consistent with Nischal et al. (2019) and Nischal (2019) who illustrated the nonmigrating semidiurnal tide signature in NO cooling rate over the latitude band ±40° for September 2013 at 125 km. Albeit the detailed propagation pathway remains unclear, SW1 and SW3 have been previously thought to arise from in-situ non-linear interaction of SW2 with QSPW1, the latter presumably generated in the mid-latitude stratosphere during austral winter and spring. An alternative mechanism is generation by the semidiurnal modulation of latent heating combined with the wavenumber 1 imparted by the surface geography, followed by upward propagation from the troposphere.

In summary, our study suggests that (i) the combined nonmigrating tides SW6 and SE2 provide an important semidiurnal modulation of the lower thermospheric NO abundance (slightly larger than the migrating tide contribution) at low latitudes, except the boreal summer. It is inducing a semidiurnal (apparent) longitudinal wave-4 in the sun-synchronous Odin/SMR NO observations during the boreal winter and spring, of similar relative magnitude as the well-studied wave-4 associated to the nonmigrating diurnal tide DE3 prevailing in the boreal summer. (ii) Further analysis of mesospheric temperatures between 50 and 95 km during the boreal winter by SMR does not reveal a corresponding wave-4 below 85 km, suggesting that the nonmigrating semidiurnal wave-4 tide may be generated in-situ in the MLT rather than propagating up from the troposphere. (iii) At subtropical latitudes, the apparent wave-1 is the more important contributor during many months especially in the southern hemisphere (e.g. March and May-to-October at −30°).

We iterate the caveat that June–July measurements are limited to 6 years (see Section 2). The limited climatology and the distribution of pair time-separation departing from 12 h does not allow to support firm conclusions concerning an apparent wave-1 during the two months.

Finally, we have here derived the 20-year climatology of semidiurnal tides in NO, based on SMR observations. It is well-established

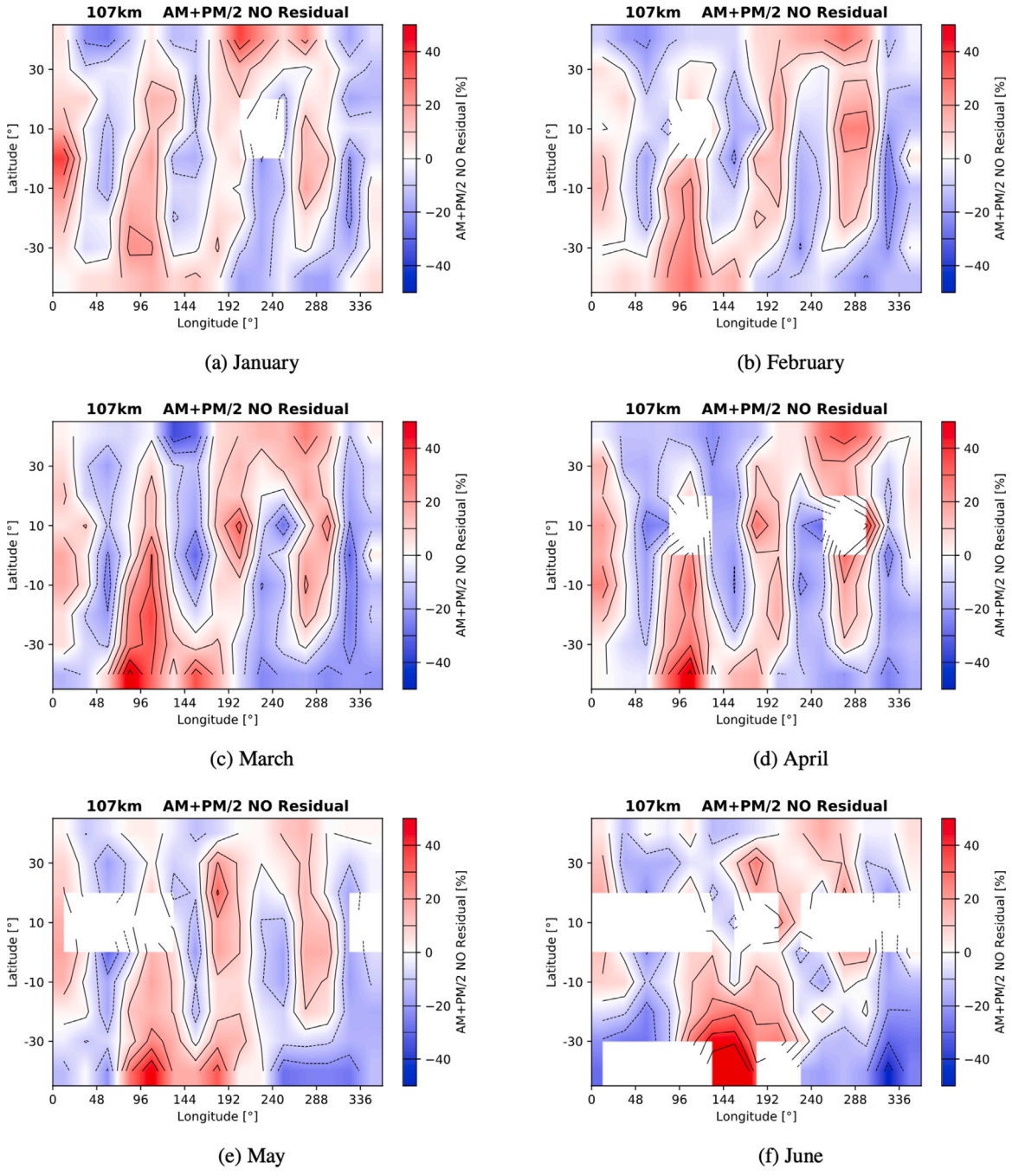


**Fig. 4.** Monthly climatologies of pair-average SMR NO residuals between −40°–+ 40° latitude at 107 km altitude.

that there is considerable interannual variability in tidal amplitudes, induced by tropospheric climate patterns modulating water vapour abundance such the El Nino/Southern Oscillation, internal stratospheric variability such as the Quasi-Biannual Oscillation, or external forcings such as the 11-year solar cycle (Kumari, 2021; Nischal et al., 2019; Nischal, 2019). The latter influences the temperature and abundance of atomic oxygen, hence the abundance of NO, and the amplitude of tides propagating from below, as the dissipation is lessened in a colder atmosphere (e.g. in solar minima). Not all these factors might manifest in NO tides however. The limited, irregular sampling by SMR (e.g., Fig. 1a) does not allow us to examine such interannual variations.

## CRediT authorship contribution statement

**Francesco Grieco:** Analyzed the satellite data, Made the calculations and the plots, Contributed to the writing of the text, Contributed to the interpretation of the results, Proofread the text, Discussions. **Yvan Orsolini:** Wrote most of the text, Contributed to the interpretation of the results, Proofread the text, Discussions. **Kristell Pérot:**

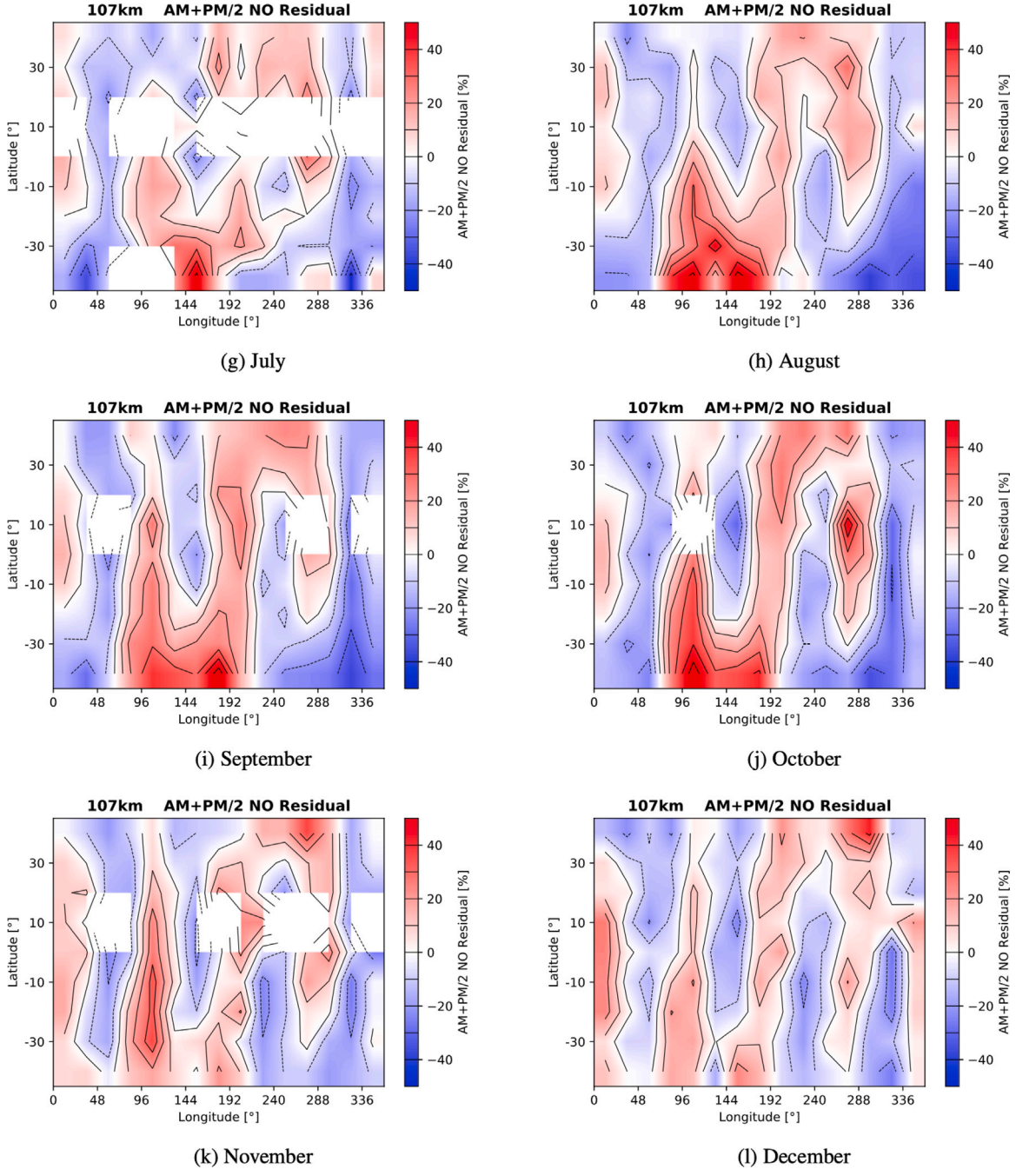


**Fig. 4.** (*continued*).

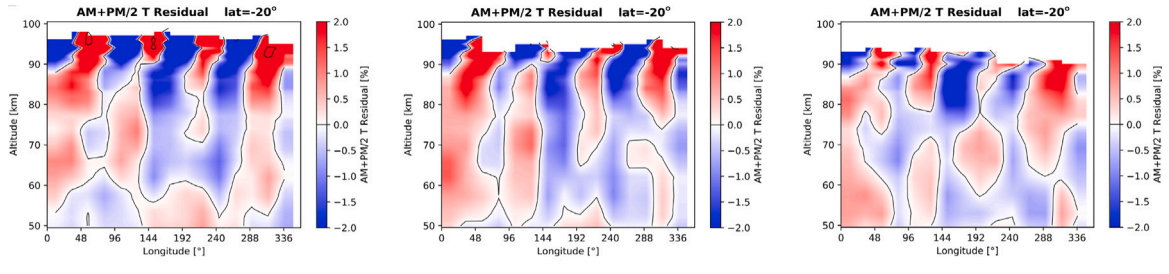


**Fig. 5.** Monthly climatologies of pair-average SMR temperature residuals at −20° latitude from 50 to 95 km in December (a), January (b) and February (c).

Contributed to the interpretation of the results, Proofread the text, Discussions, Funding acquisition.

## Declaration of competing interest

The authors declare that they have no known competing financial interests or personal relationships that could have appeared to influence the work reported in this paper.

## Data availability

Odin/SMR v3.0 L2 data are publicly accessible at http://odin.rss.chalmers.se/level2.

## Acknowledgements

Odin is a Swedish-led satellite mission, and is also part of the European Space Agency's (ESA) third party mission programme. The recent reprocessing of the SMR NO data was supported by ESA and by the Swedish National Space Agency (SNSA, Dnr 20/88). The authors acknowledge additional support from SNSA (Dnr 20/178), and are grateful to Dr. Robert Hibbins for his invaluable comments on an early version of this paper.

## References

Bermejo-Pantaleón, D., Funke, B., López-Puertas, M., García-Comas, M., Stiller, G.P., von Clarmann, T., Linden, A., Grabowski, U., Höpfner, M., Kiefer, M., Glatthor, N., Kellmann, S., Lu, G., 2011. Global observations of thermospheric temperature and nitric oxide from MIPAS spectra at 5.3 μm. J. Geophys. Res. Space Phys. 116 (A10), http://dx.doi.org/10.1029/2011JA016752, URL: https://agupubs.onlinelibrary.wiley.com/doi/abs/10.1029/2011JA016752.

Bruinsma, S.L., Forbes, J.M., 2010. Large-scale traveling atmospheric disturbances (LSTADs) in the thermosphere inferred from CHAMP, GRACE, and SETA accelerometer data. J. Atmos. Sol.-Terr. Phys. 72 (13), 1057–1066. http://dx.doi.org/10.1016/j.jastp.2010.06.010, URL: https://www.sciencedirect.com/science/article/pii/S1364682610001860.

Eriksson, P., 1999. Microwave Radiometric Observations of the Middle Atmosphere: Simulations and Inversions. (Ph.D. thesis). Chalmers University of Technology.

Forbes, J.M., Oberheide, J., Zhang, X., Cullens, C., Englert, C.R., Harding, B.J., Harlander, J.M., Marr, K.D., Makela, J.J., Immel, T.J., 2022. Vertical coupling by solar semidiurnal tides in the thermosphere from ICON/MIGHTI measurements. J. Geophys. Res. Space Phys. 127 (5), e2022JA030288. http://dx.doi.org/10.1029/2022JA030288, URL: https://agupubs.onlinelibrary.wiley.com/doi/abs/10.1029/2022JA030288, e2022JA030288 2022JA030288.

Frisk, U., Hagström, M., Ala-Laurinaho, J., Andersson, S., Berges, J.-C., Chabaud, J.-P., Dahlgren, M., Emrich, A., Florén, H.-G., Florin, G., Fredrixon, M., Gaier, T., Haas, R., Hirvonen, T., Hjalmarsson, A., Jakobsson, B., Jukkala, P., Kildal, P.S., Kollberg, E., Lassing, J., Lecacheux, A., Lehikoinen, P., Lehto, A., Mallat, J., Marty, C., Michet, D., Narbonne, J., Nexon, M., Olberg, M., Olofsson, A.O.H., Olofsson, G., Origné, A., Petersson, M., Piironen, P., Pons, R., Pouliquen, D., Ristorcelli, I., Rosolen, C., Rouaix, G., Räisänen, A.V., Serra, G., Sjöberg, F., Stenmark, L., Torchinsky, S., Tuovinen, J., Ullberg, C., Vinterhav, E., Wadefalk, N., Zirath, H., Zimmermann, P., Zimmermann, R., 2003. The Odin satellite I. Radiometer design and test. Astron. Astrophys. 402 (3), L27–L34. http://dx.doi.org/10.1051/0004-6361:20030335.

García-Comas, M., González-Galindo, F., Funke, B., Gardini, A., Jurado-Navarro, A., López-Puertas, M., Ward, W.E., 2016. MIPAS observations of longitudinal oscillations in the mesosphere and the lower thermosphere: climatology of odd-parity daily frequency modes. Atmos. Chem. Phys. 16 (17), 11019–11041. http://dx.doi.org/10.5194/acp-16-11019-2016, URL: https://acp.copernicus.org/articles/16/11019/2016/.

Hagan, M.E., Forbes, J.M., 2003. Migrating and nonmigrating semidiurnal tides in the upper atmosphere excited by tropospheric latent heat release. J. Geophys. Res. Space Phys. 108 (A2), http://dx.doi.org/10.1029/2002JA009466, URL: https://agupubs.onlinelibrary.wiley.com/doi/abs/10.1029/2002JA009466.

He, M., Chau, J.L., Stober, G., Hall, C.M., Tsutsumi, M., Hoffmann, P., 2017. Application of manley-rowe relation in analyzing nonlinear interactions between planetary waves and the solar semidiurnal tide during 2009 sudden stratospheric warming event. J. Geophys. Res. Space Phys. 122 (10), 10,783–10,795. http://dx.doi.org/10.1002/2017JA024630, URL: https://agupubs.onlinelibrary.wiley.com/doi/abs/10.1002/2017JA024630.

Kiviranta, J., Pérot, K., Eriksson, P., Murtagh, D., 2018. An empirical model of nitric oxide in the upper mesosphere and lower thermosphere based on 12 years of Odin SMR measurements. Atmos. Chem. Phys. 18 (18), 13393–13410. http://dx.doi.org/10.5194/acp-18-13393-2018, URL: https://acp.copernicus.org/articles/18/13393/2018/.

Kumari, K., 2021. Short-Term Variability of Atmospheric Tides in Earth's Mesosphere and Lower Thermosphere Region. (Ph.D. thesis). Clemson University.

Lieberman, R.S., 1991. Nonmigrating diurnal tides in the equatorial middle atmosphere. J. Atmos. Sci. 48 (8), 1112–1123. http://dx.doi.org/10.1175/1520-0469(1991)048<1112:NDTITE>2.0.CO;2.

Liu, G., Janches, D., Lieberman, R.S., 2018. Intraseasonal variations of nonmigrating tides observed near the mesopause. J. Geophys. Res. Space Phys. 123 (11), 9921–9931. http://dx.doi.org/10.1029/2018JA025709, URL: https://agupubs.onlinelibrary.wiley.com/doi/abs/10.1029/2018JA025709.

Marsh, D.R., Russell III, J.M., 2000. A tidal explanation for the sunrise/sunset anomaly in haloe low-latitude nitric oxide observations. Geophys. Res. Lett. 27 (19), 3197–3200. http://dx.doi.org/10.1029/2000GL000070, URL: https://agupubs.onlinelibrary.wiley.com/doi/abs/10.1029/2000GL000070.

McLandress, C., Ward, W.E., 1994. Tidal/gravity wave interactions and their influence on the large-scale dynamics of the middle atmosphere: Model results. J. Geophys. Res.: Atmos. 99 (D4), 8139–8155. http://dx.doi.org/10.1029/94JD00486, URL: https://agupubs.onlinelibrary.wiley.com/doi/abs/10.1029/94JD00486.

Nischal, N., 2019. Nonmigrating Tidal Impact on the Energy Budget of the Lower Thermosphere. (Ph.D. thesis). Clemson University.

Nischal, N., Oberheide, J., Mlynczak, M.G., Marsh, D.R., Gan, Q., 2019. Solar cycle variability of nonmigrating tides in the 5.3 and 15 μm infrared cooling of the thermosphere (100–150 km) from SABER. J. Geophys. Res. Space Phys. 124 (3), 2338–2356. http://dx.doi.org/10.1029/2018JA026356, URL: https://agupubs.onlinelibrary.wiley.com/doi/abs/10.1029/2018JA026356.

Oberheide, J., Forbes, J.M., 2008. Thermospheric nitric oxide variability induced by nonmigrating tides. Geophys. Res. Lett. 35 (16), http://dx.doi.org/10.1029/2008GL034825, URL: https://agupubs.onlinelibrary.wiley.com/doi/abs/10.1029/2008GL034825.

Oberheide, J., Forbes, J.M., Zhang, X., Bruinsma, S.L., 2011. Wave-driven variability in the ionosphere-thermosphere-mesosphere system from TIMED observations: What contributes to the "wave 4"? J. Geophys. Res. Space Phys. 116 (A1), http://dx.doi.org/10.1029/2010JA015911, URL: https://agupubs.onlinelibrary.wiley.com/doi/abs/10.1029/2010JA015911.

Oberheide, J., Hagan, M., Richmond, A., Forbes, J., 2015. DYNAMICAL meteorology | atmospheric tides. In: North, G.R., Pyle, J., Zhang, F. (Eds.), Encyclopedia of Atmospheric Sciences, second ed. Academic Press, Oxford, pp. 287–297. http://dx.doi.org/10.1016/B978-0-12-382225-3.00409-6, URL: https://www.sciencedirect.com/science/article/pii/B9780123822253004096.

Oberheide, J., Hagan, M.E., Roble, R.G., Offermann, D., 2002. Sources of nonmigrating tides in the tropical middle atmosphere. J. Geophys. Res.: Atmos. 107 (D21), ACL 6–1–ACL 6–14. http://dx.doi.org/10.1029/2002JD002220, URL: https://agupubs.onlinelibrary.wiley.com/doi/abs/10.1029/2002JD002220.

Oberheide, J., Mlynczak, M.G., Mosso, C.N., Schroeder, B.M., Funke, B., Maute, A., 2013. Impact of tropospheric tides on the nitric oxide 5.3 μm infrared cooling of the low-latitude thermosphere during solar minimum conditions. J. Geophys. Res. Space Phys. 118 (11), 7283–7293. http://dx.doi.org/10.1002/2013JA019278, URL: https://agupubs.onlinelibrary.wiley.com/doi/abs/10.1002/2013JA019278.

Pancheva, D., Merzlyakov, E., Mitchell, N., Portnyagin, Y., Manson, A., Jacobi, C., Meek, C., Luo, Y., Clark, R., Hocking, W., MacDougall, J., Muller, H., Kürschner, D., Jones, G., Vincent, R., Reid, I., Singer, W., Igarashi, K., Fraser, G., Fahrutdinova, A., Stepanov, A., Poole, L., Malinga, S., Kashcheyev, B., Oleynikov, A., 2002. Global-scale tidal variability during the PSMOS campaign of June–August 1999: interaction with planetary waves. J. Atmos. Sol.-Terr. Phys. 64 (17), 1865–1896. http://dx.doi.org/10.1016/S1364-6826(02)00199-2, URL: https://www.sciencedirect.com/science/article/pii/S1364682602001992.

Pérot, K., Orsolini, Y.J., 2021. Impact of the major SSWs of february 2018 and january 2019 on the middle atmospheric nitric oxide abundance. J. Atmos. Sol.-Terr. Phys. 218, 105586. http://dx.doi.org/10.1016/j.jastp.2021.105586, URL: https://www.sciencedirect.com/science/article/pii/S136468262100047X.

Ren, Z., Wan, W., Xiong, J., Li, X., 2020. A simulation of the influence of DE3 tide on nitric oxide infrared cooling. J. Geophys. Res. Space Phys. 125 (3), e2019JA027131. http://dx.doi.org/10.1029/2019JA027131, URL: https://agupubs.onlinelibrary.wiley.com/doi/abs/10.1029/2019JA027131, e2019JA027131 2019JA027131.

Sakazaki, T., Sato, K., Kawatani, Y., Watanabe, S., 2015. Three-dimensional structures of tropical nonmigrating tides in a high-vertical-resolution general circulation model. J. Geophys. Res.: Atmos. 120 (5), 1759–1775. http://dx.doi.org/10.1002/2014JD022464, URL: https://agupubs.onlinelibrary.wiley.com/doi/abs/10.1002/2014JD022464.

Salinas, C.C.J.H., Wu, D.L., Lee, J.N., Chang, L.C., Qian, L., Liu, H., 2023. Seasonality of the migrating semidiurnal tide in the tropical upper mesosphere and lower thermosphere and its thermodynamic and momentum budget. J. Geophys. Res. Space Phys. 128 (2), e2022JA031035. http://dx.doi.org/10.1029/2022JA031035, URL: https://agupubs.onlinelibrary.wiley.com/doi/abs/10.1029/2022JA031035, e2022JA031035 2022JA031035.

Siskind, D.E., Barth, C.A., Russell, III, J.M., 1998. A climatology of nitric oxide in the mesosphere and thermosphere. Adv. Space Res. 21 (10), 1353–1362. http://dx.doi.org/10.1016/S0273-1177(97)00743-6.

Siskind, D.E., Jones, Jr., M., Drob, D.P., McCormack, J.P., Hervig, M.E., Marsh, D.R., Mlynczak, M.G., Bailey, S.M., Maute, A., Mitchell, N.J., 2019. On the relative roles of dynamics and chemistry governing the abundance and diurnal variation of low-latitude thermospheric nitric oxide. Ann. Geophys. 37 (1), 37–48. http://dx.doi.org/10.5194/angeo-37-37-2019, URL: https://angeo.copernicus.org/articles/37/37/2019/.

Smith, A.K., Pancheva, D.V., Mitchell, N.J., 2004. Observations and modeling of the 6-hour tide in the upper mesosphere. J. Geophys. Res.: Atmos. 109 (D10), http://dx.doi.org/10.1029/2003JD004421, URL: https://agupubs.onlinelibrary.wiley.com/doi/abs/10.1029/2003JD004421.

Truskowski, A., Forbes, J., Zhang, X., Palo, S., 2014. New perspectives on thermosphere tides: 1. Lower thermosphere spectra and seasonal-latitudinal structures. Earth Planets Space 66, 136. http://dx.doi.org/10.1186/s40623-014-0136-4.

Zhang, X., Forbes, J.M., Hagan, M.E., Russell III, J.M., Palo, S.E., Mertens, C.J., Mlynczak, M.G., 2006. Monthly tidal temperatures 20–120 km from TIMED/SABER. J. Geophys. Res. Space Phys. 111 (A10), http://dx.doi.org/10.1029/2005JA011504, URL: https://agupubs.onlinelibrary.wiley.com/doi/abs/10.1029/2005JA011504.

Zhang, J., Limpasuvan, V., Orsolini, Y.J., Espy, P.J., Hibbins, R.E., 2021. Climatological westward-propagating semidiurnal tides and their composite response to sudden stratospheric warmings in SuperDARN and SD-WACCM-X. J. Geophys. Res.: Atmos. 126 (3), e2020JD032895. http://dx.doi.org/10.1029/2020JD032895, URL: https://agupubs.onlinelibrary.wiley.com/doi/abs/10.1029/2020JD032895, e2020JD032895 2020JD032895.